Mode characteristics of VCSELs with different shape and size oxidation apertures

Xin-Yu Xie(谢新宇)[1,2], Jian Li(李健)[1,2], Xiao-Lang Qiu(邱小浪)[1,2], Yong-Li Wang(王永丽)[1,2], Chuan-Chuan Li(李川川)[1,2,†], and Xin Wei(韦欣)[1,2]

[1] *Institute of Semiconductors, Chinese Academy of Sciences, Beijing* 100083, *China*
[2] *Center of Materials Science and Optoelectronics Engineering, University of Chinese Academy of Sciences, Beijing* 100049, *China*

(Received 4 August 2022; revised manuscript received 21 September 2022; accepted manuscript online 7 October 2022)

Vertical cavity surface emitting laser (VCSELs) as the ideal light source for rubidium (Rb) and cesium (Cs) atomic clocks is analyzed for its mode and polarization control. We fabricated three kinds of shapes: triangular, elliptic, and circular oxidation apertures which also have different sizes. We formed three different shape oxide apertures by wet-oxidation with 36 μm–39 μm circular mesa. Our results show that triangular oxidized-VCSEL has the advantages of mode and polarization selection over elliptic and circular oxide apertures. When triangular oxide-confined VCSELs emit in single mode, the measured side mode suppression ratio (SMSR) is larger than 20 dB and orthogonal polarization suppression ratio achieves 10 dB. Resonant blueshift of VCSELs with triangular and elliptic apertures is observed with the decrease of aperture size.

Keywords: semiconductor lasers, laser diodes, microcavity and microdisk lasers, semiconductor-device characterization, design, modeling

PACS: 42.55.Px, 42.55.Sa, 85.30.De **DOI:** 10.1088/1674-1056/ac9821

1. Introduction

Vertical-cavity surface-emitting lasers (VCSELs) are attractive for many applications due to its low threshold current, single longitudinal mode, ease of current modulation with RF signals, low power consumption. Atomic clocks are main tools of precise time measurement. VCSELs are ideal light source for Cs and Rb chip-scale atomic clocks (CSAC) based on coherent population trapping (CPT) effect, which requiring VCSEL of single mode and polarization orientation. VCSEL has single longitudinal mode essentially for its short cavity on vertical direction. When we discuss single mode VCSEL, it means single transverse mode. There are some methods of mode control, such as surface relief,[1] proton-implanted,[2] photonic crystal VCSELs,[3] oxidation aperture.[2,4] In oxide-confined VCSELs with proton-implanted, when oxidation apertures decrease to 3 μm–5 μm, VCSELs operate at fundamental mode.[2,4] However, series resistance can be increased by small aperture size. Generally, VCSELs have two orthogonal polarization modes because of isotropic gain, which coexist and align primarily along the [011] and [0-11] crystal axes.[5] There have been a number of efforts to achieve polarization control in VCSELs, including utilizing an asymmetrical mesa structure,[6] growing VCSELs on misoriented substrate,[7] mode and polarization selecting gratings,[8] *etc.* There is also a method using rhomboidal aperture to realize polarization control. In Ref. [9], the authors proposed a kind of VCSEL with rhomboidal oxidation aperture that minor diagonal is the direction of radiation polarization.

The influence of wet oxidation process parameters such as gas flow, gas composition, temperature, Al composition, and layer thickness on the rate of oxidation rate have been studied in Ref. [10]. In the authentic fabrication process, there are some deviations of these parameters. Therefore, VCSEL's oxidation aperture could be other shape even if mesa is circular. In Ref. [11], the authors obtained a rectangular and circular aperture by changing the Al content and mesa shape.

We fabricated three kinds of VCSELs with different oxidation apertures in shape. In this paper, we present the results of simulations and experiments about emission spectrum and polarization selection. Our results show that triangular oxidation aperture is superior to elliptic and circular apertures in the mode and polarization control with the same aperture size. VCSELs with 6.2-μm side triangular oxidation aperture can emit in single mode, while SMSR is 26 dB with 4-μm side and OPSR can reach 10 dB with 5.4-μm side.

2. Simulation

The finite difference time domain (FDTD) method is widely used to analyze optical phenomenon. We utilize FDTD methods to analyze the influence of different shape oxidation apertures on the emission spectrum and polarization. Polarization controlling is analyzed by comparing power of two orthogonal polarization source setting. The structure of VCSEL is built in the FDTD solver region, as shown in Fig. 1. We use plane wave as source of simulation. TE plane wave is characterized by setting polarization angle at 0°, and TM plane wave

[†]Corresponding author. E-mail: lichuan@semi.ac.cn

© 2023 Chinese Physical Society and IOP Publishing Ltd

polarization angle is 90°. The boundary condition set *x*-min as symmetric when polarization orientation is tangential to the *x*-min boundary, otherwise it should be anti-symmetric at *x*-min. As to elliptic aperture and circular aperture, symmetric and anti-symmetric boundary conditions are used at *x*-min and *y*-min according to the setting up of the source.

Table 1. Energy flow density of different aperture shapes and sizes in same area.

Triangle (μm)	TE	TM	Circle (μm)	TE	TM	Ellipse (μm)	TE	TM
4	1.1924	0.677	4	0.8937	0.916	8–5.4	0.9917	0.999
5.4	0.6492	0.8979	5	0.8166	0.8355	9–5.4	1.0644	1.0771
6.2	0.7582	0.7662	6	1.1512	1.1518	10–6	1.1221	1.0808
7.5	0.0248	1.1677	7	0.8979	0.9204	10–7	1.2112	1.1689

The *E*-distribution of triangular, elliptic, and circular apertures in light-emitting face and cross-section are calculated by the superposition of all recorded wavelength as shown in Fig. 2. The OPSR is obtained by exporting the power distribution of TE and TM waves in the frequency field and the power monitor. As we can see in Table 1 and Fig. 2, triangular oxide apertures are of benefit for polarization selection and have more restriction on transverse mode than the other two shapes.

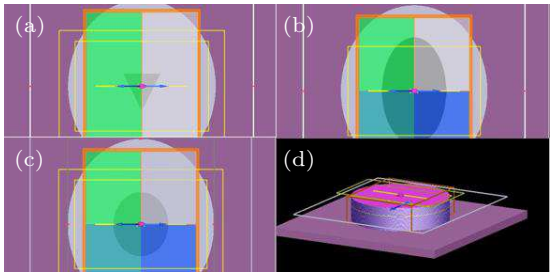


Fig. 1. Panels (a)–(d) are the FDTD simulation model.

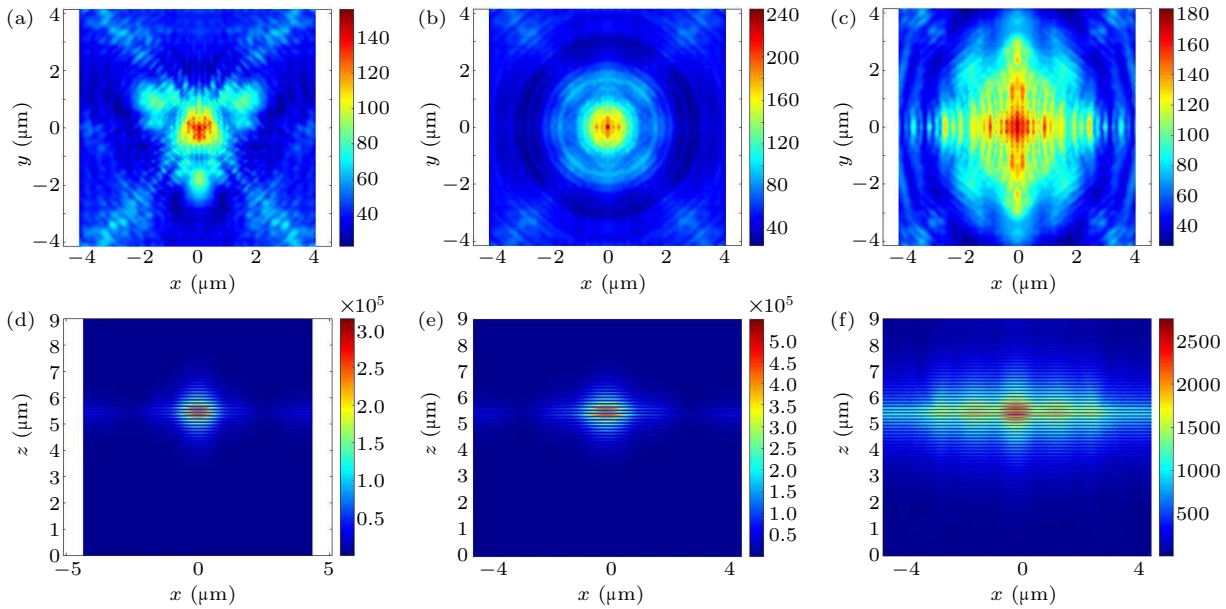


Fig. 2. Panels (a)–(c) are the *E*-distributions on emitting surface of triangular, circular, and elliptic oxide-confined VCSELs with 5.4 μm, 5 μm, and 9 μm–5.4 μm aperture sizes respectively. Panels (d)–(e) are the *E*-distributions on cross-section, the sorting is the same as the former.

3. Fabrication of VCSELs

Our VCSELs are composed of top and bottom distributed Bragg reflectors (DBRs), active-region, $Al_{0.98}Ga_{0.02}As$ oxidation layer. DBRs contains 22 pairs and 35 pairs of quarter-wave $Al_{0.2}Ga_{0.8}As/Al_{0.9}Ga_{0.1}As$. $Al_{0.98}Ga_{0.02}As$ oxidation layer is 30 nm grown on the top of λ-cavity. The VCSEL structure is fabricated by metal–organic chemical vapor deposition (MOCVD). After epitaxy, we carried out lateral wet-oxidation. By changing the oxidation condition, we obtained three different shape oxidation apertures, including triangle, ellipse, and circle. Figure 3 shows images of triangular and elliptic oxidation apertures.

We measured the side of equilateral triangle oxidation apertures C1, C2, C3, C4 = 4 μm, 5.4 μm, 6.2 μm, 7.5 μm. And elliptic apertures have major axes a1, a2, a3, a4 = 8 μm, 9 μm, 10 μm, 10 μm and minor axes b1, b2, b3, b4 = 5.4 μm, 5.4 μm, 6 μm, 7 μm. The four pairs of elliptic aperture sizes are marked as B1, B2, B3, B4. With respect to circular apertures, their diameters A1, A2, A3, A4 are 4 μm, 5 μm, 6 μm, 7 μm. We use 1, 2 ,3 represent circular, elliptic, and triangular apertures respectively.

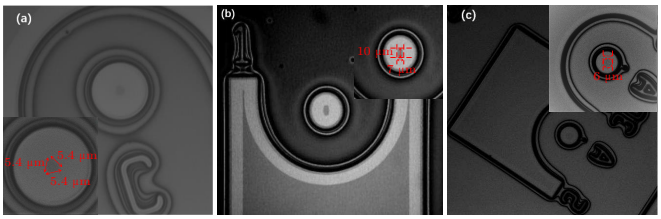


Fig. 3. (a) Triangular oxidation aperture, (b) elliptic oxidation aperture, (c) circular aperture. The inset images of panels (a)–(c) are specific parameters of apertures.

4. Experiments and results

The measurement of VCSELs' spectrum is taken by coupling output light into multi-mode fiber and analyzed by spectroscope as shown in Fig. 4. When triangle oxide aperture VCSEL emits with single mode, and the SMSR can reach 26 dB at 4-μm oxidation aperture. At the same time, the circular aperture VCSEL has 2 peaks, and the elliptic VCSEL has 3 peaks. For triangular aperture, we have 4 μm, 5.4 μm, 6.2 μm, and 7.5 μm sides of triangle aperture, and the single peak laser output is maintained all the time. Meanwhile the full width at half maximum (FWHM) of VCSEL with triangular apertures can reach 0.124 nm. We can obtain that the triangular oxidation aperture is more advantageous for mode selecting than elliptic and circular apertures. According to the simulation above, we attribute it to the stronger suppression effect of the triangular aperture on higher-order modes than the other two. And the peak wavelength increases along with the increase of the oxidation aperture size under the same injection current.

Resonant-mode blueshift with the shrink of the aperture size can be observed in the spectrums of triangular and elliptic oxide-apertured VCSELs, as shown in Fig. 5. This phenomenon is compatible with the theory proposed by Noble, *et al.* This blueshift results because small cavities transform the lasing mode from plane wave into a true three-dimensional mode. Cylindrical weighted-index-model and effective aperture radius are adopted in the calculation of square aperture.[12] The effective aperture radius is calculated in Table 2. Moreover, r_{eff1}, r_{eff2}, r_{eff3} are the effective aperture radii of circular, elliptic, and triangular apertures. And we calculated central wavelength λ_{c} of multi-mode by the following equation taking reference to the method of finding FBG central wavelength[13]

$$\lambda_{\mathrm{c}} = \frac{\sum_{i=1}^{N} \lambda_i I_i}{\sum_{i=1}^{N} I_i}, \tag{1}$$

where N is the number of modes, λ_i is the wavelength of the i-th peak in the spectrum and I_i is the intensity of the i-th peak. It has to be noted that current gathering occurs in the corner of triangular oxidation aperture and the edge of major-axes of elliptic aperture which are similar to rhomboidal apertures.[9] With the decrease of size of triangle and ellipse apertures, the current density increases at the angle and edge where high-order mode locates, leading to arising of temperature, but central transverse-modes are still not influenced by it. Different from other two shapes, the current of circular aperture converges in the central area of aperture. The temperatures of the center increase as the shrink of aperture size because of the rise of current density.

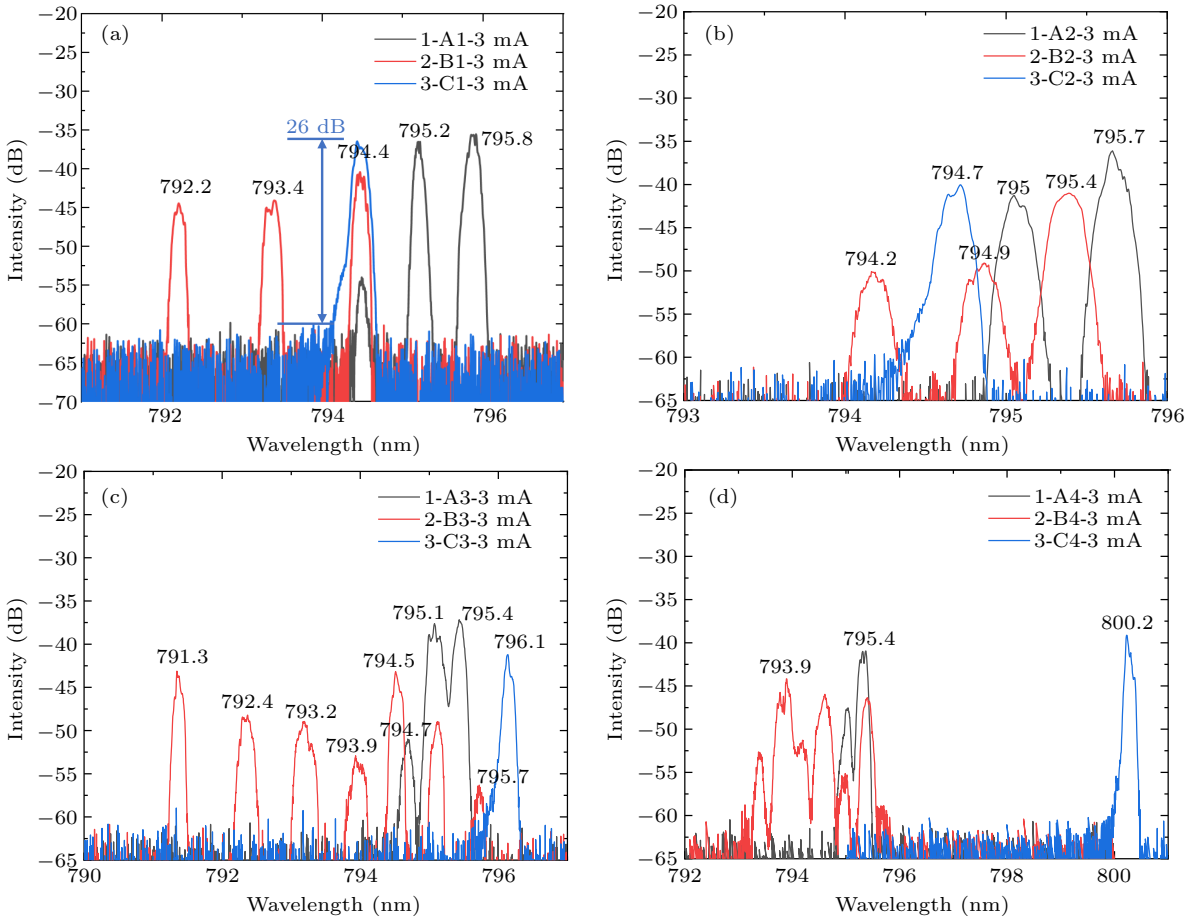


Fig. 4. Spectrums of VCSELs with oxidation aperture shapes 1–3 and aperture sizes A1–A4, B1–B4, C1–C4 respectively.

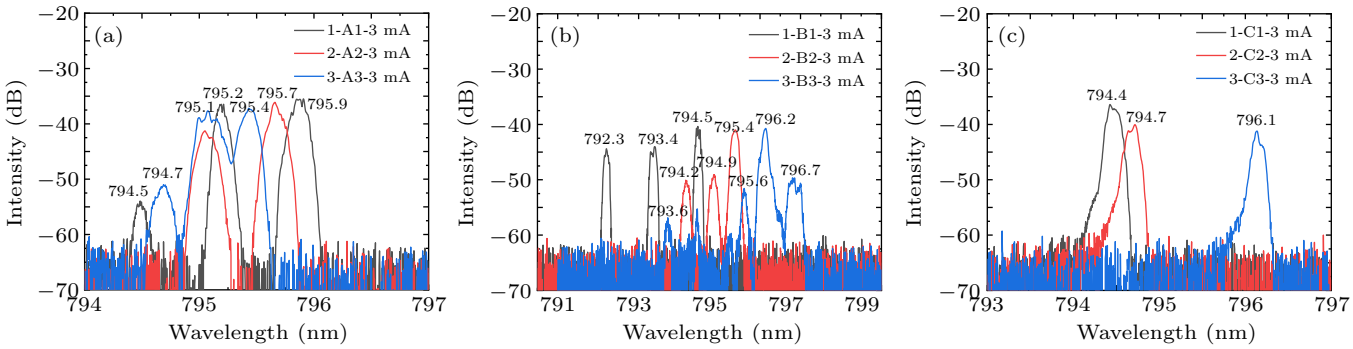


Fig. 5. The spectrums of VCSELs with different aperture shapes with the increase of aperture size at 3-mA current. 1: circle aperture, 2: ellipse aperture, 3: triangle aperture. A1–A3, B1–B3, and C1–C4 are aperture sizes.

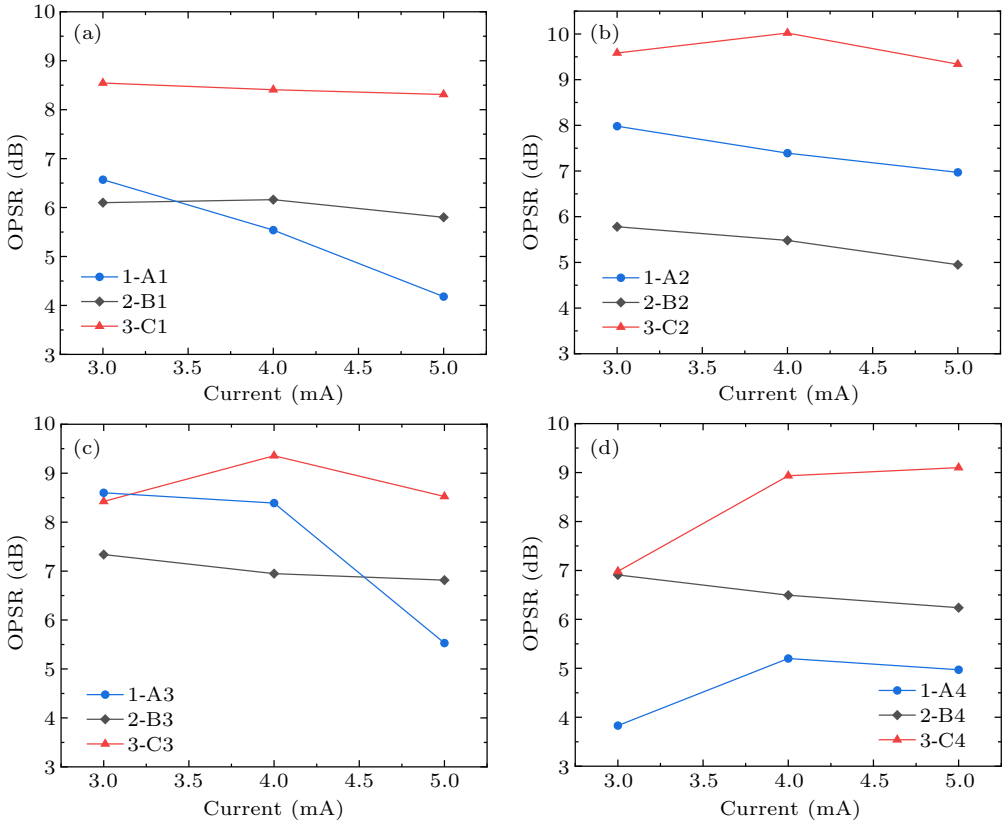


Fig. 6. OPSR–current of different aperture shapes and different sizes respectively. 1: circle, 2: ellipse, 3: triangle. A1–A4, B1–B4, and C1–C4 mean different aperture sizes.

Table 2. The effective aperture radius of different aperture shapes and aperture sizes.

1-aperture size (μm)	r_{eff1} (μm)	λ_c (nm)	2-aperture size (μm)	r_{eff2} (μm)	λ_c (nm)	3-aperture size (μm)	r_{eff3} (μm)	λ_c (nm)
4	2	795.46	8–5.4	3.29	793.51	4	1.49	794.4
5	2.5	795.45	9–5.4	3.49	794.94	5.4	2.00	794.7
6	3	795.25	10–6	3.87	795.85	6.2	2.30	796.1

We take maximum power tests of these VCSELs at room temperature on wafer, as shown in Table 3 which gives normalized power of VCSELs with different aperture shapes at different sizes. The power of VCSELs with elliptic aperture is the largest among these three kinds of VCSELs because its effective radius is larger than the other two shapes, and so the VCSEL with triangular apertures is the lowest.

The *P*–*I* characteristics of three types of VCSELs at different sizes are shown in Figs. 6(a)–6(d). The power ratio of the polarization is measured by adding a polarizer above top of the VCSEL. We calculated OPSR described by the following equation:

$$\text{OPSR} = 10\log_{10} P_{\max}/P_{\min}. \tag{2}$$

We analyzed the influence of shape and size of aperture on polarizations. Moreover, all these data were obtained by aver-

aging the value of original data which measured by more than 5 samples. As we can see in Fig. 6, the triangular oxidation aperture is more useful for polarization control than the other two shapes, while it can reach 10.5 dB and larger than 7 dB. We attributed it to the lateral optical confinement of the triangle aperture. And there is not much difference in polarization control between ellipse-aperture and circle-aperture.

Table 3. normalized power of VCSELs with different aperture shapes at different sizes.

1-aperture size (μm)	P_N	2-aperture size (μm)	P_N	3-aperture size (μm)	P_N
4	0.499	8–5.4	0.828	4	0.325
5	0.54	9–5.4	0.864	5.4	0.368
6	0.677	10–6	0.944	6.2	0.397
7	0.71	10–7	1	7.5	0.454

5. Conclusion

In this paper, we have fabricated VCSELs with circular, elliptic, and triangular oxide apertures. We simulated and measured the mode and polarization characteristics of the three types of VCSELs. In the same mesa size, it is obvious that the triangular aperture is more beneficial to mode and polarization selections compared with elliptic and circular apertures. And resonant-mode blueshift of VCSELs with triangular and elliptic apertures is observed while aperture size is decreased at 3 mA. Meanwhile, the redshift of VCSELs with circular aperture at 3 mA is attributed to the arise of temperatures.

References

[1] Gadallah A and Michalzick R 2011 *IEEE Photon. Technol. Lett.* **23** 1040

[2] ChangHasnain C J, Orenstein M, Lehmen A V, *et al.* 1990 *Appl. Phys. Lett.* **57** 218

[3] Cao T, Xu C, Xie Y Y, *et al.* 2013 *Chin. Phys. B* **22** 024205

[4] Jung C, Jager R, Grabherr M, *et al.* 1997 *Electron. Lett.* **33** 1790

[5] Rao Z, Matteo J A, Hesselink L, *et al.* 2007 *Appl. Phys. Lett.* **90** 191110

[6] Yoshikawa T, Kosaka H, Kurihara K, *et al.* 1995 *Appl. Phys. Lett.* **66** 908

[7] Takahashi M and Vaccaro P 1996 *IEEE Photon. Technol. Lett.* **8** 737

[8] Hauglund E, Jahed M, Gustavsson J S, *et al.* 2019 *Opt. Express* **27** 18892

[9] Bobrov M A, Maleev N A, Blokhin S A, *et al.* 2016 *Semiconductors* **50** 1390

[10] Geib K, Choquette K, Hou H, *et al.* 1997 *Photonics West* 97, April 4, **3003**

[11] Choquette K D, Geib K M, Ashby C I H, *et al.* 1997 *IEEE J. Select. Top. Quantum Electron.* **3** 916

[12] Noble M J, Shin J H, Choquette K D, Lott J A and Lee Y H 2001 *IEEE Photon. Technol. Lett.* **10** 475

[13] Zhao Y, Zhang W F, Zhang M, *et al.* (C.N. Patent) 109884080A [2019-09-14]